PAPER • OPEN ACCESS

Wells turbine efficiency improvements: experimental application of a speed control strategy

To cite this article: Fabio Licheri *et al* 2022 *J. Phys.: Conf. Ser.* **2385** 012132

View the article online for updates and enhancements.

You may also like

- PARTICLE-IN-CELL SIMULATION OF A STRONG DOUBLE LAYER IN A NONRELATIVISTIC PLASMA FLOW: ELECTRON ACCELERATION TO ULTRARELATIVISTIC SPEEDS
Mark E. Dieckmann and Antoine Bret
- Review of laser-driven ion sources and their applications
Hiroyuki Daido, Mamiko Nishiuchi and Alexander S Pirozhkov
- Liquid-based electrostatic energy harvester with high sensitivity to human physical motion
Dong-Hoon Choi, Chang-Hoon Han, Hyun-Don Kim et al.

This content was downloaded from IP address 192.167.140.186 on 11/01/2023 at 12:22

Wells turbine efficiency improvements: experimental application of a speed control strategy

Fabio Licheri*, Tiziano Ghisu, Francesco Cambuli, Pierpaolo Puddu
Department of Mechanical, Chemical and Materials Engineering, University of Cagliari, Italy
E-mail: fabio.licheri@unica.it

Abstract. Systems based on the OWC principle allow to convert the sea-wave energy into electrical energy. The potential energy contained in the wave motion is first converted into the pneumatic energy of a bi-directional airflow, generated by the oscillatory displacement of a column of water inside a chamber. Then, an air turbine, such as the Wells turbine, placed at the top of the chamber, converts the pneumatic energy into mechanical energy at its shaft, which can be coupled to an electric motor to produce energy. The turbine's performance is strongly affected by the non-stationary behavior of the airflow, which continuously changes its intensity. Control solutions based on the variation of the turbine rotational speed can overcome this limitation.

This work aims to study a speed-controlled Wells turbine with an experimental approach, making use of a turbine coupled to an Oscillating Water Column (OWC) simulator. A control law for the rotational speed has been defined and applied to the turbine in order to move the turbine's operating conditions as close as possible to its maximum efficiency point, for the majority of the piston period.

The experimental results prove the effectiveness of the proposed control strategy for moving the operating conditions and for obtaining operating conditions close to the best efficiency point for the majority of the wave period.

Acronyms

BDC	bottom dead center
OWC	Oscillating Water Column
PTO	Power Take Off
TDC	top dead center

Dimensional properties

c	blade chord
C_z	flow velocity
D	turbine diameter
Δp	static pressure drop across the rotor
E	energy in a cycle
n	rotational speed
Ω	angular rotational frequency
T_w	piston period
p	static pressure
Q	volumetric flow rate
r	turbine radius
ρ	air density
t	time
T	torque
U	rotor speed
z	piston position

Non-dimensional properties

η	overall efficiency
ν	hub-to-tip ratio
ϕ	non-dimensional flow coefficient
p^*	non-dimensional static pressure drop
r^*	non-dimensional turbine radius
T^*	non-dimensional torque
Z^*	non-dimensional piston position

Subscripts and superscripts

a	available

Content from this work may be used under the terms of the Creative Commons Attribution 3.0 licence. Any further distribution of this work must maintain attribution to the author(s) and the title of the work, journal citation and DOI.
Published under licence by IOP Publishing Ltd

hub	turbine hub	*tip*	turbine tip
ref	reference value	*u*	useful

1. Introduction

Among the different sources of renewable energy, sea-wave energy is considered as one of the most attractive [1] due to its good predictability and high availability. Systems based on the Oscillating Water Column (OWC) principle are simple and reliable solutions to harvest sea-wave energy, also thanks to their flexibility to be installed at different distances from the shoreline [2, 3], hence for the reduced environmental impact.

An OWC system is generally composed of two main sections: 1) a chamber, opened on the bottom and partially submerged under the free sea surface, whose oscillation produces an alternative airflow at the top of the chamber; 2) a Power-Take-Off (PTO), which converts the pneumatic energy into mechanical energy at a shaft (hence in electric energy, by means of an electric machine). An air turbine is typically employed as a PTO, although the bi-directional nature of the airflow inside an OWC represents a challenge for the machine selection. The Wells turbine [4] overcomes this limitation, due to its symmetric blade profiles staggered at 90 degrees with respect to the axis of rotation, which allow the turbine to rotate in the same direction regardless of the flow direction. The simplicity of construction of the Wells turbine has attracted a number of authors [5, 6, 7], who have investigated its operation in order to overcome the main drawbacks of this uncommon turbomachine [8]. The most important one is probably related to the unsteady bi-directional nature of the airflow, that submits the turbine to continuously varying operating conditions and does not allow the turbine to operate at its best efficiency point [9]. A reliable solution to control the operating conditions of the Wells turbine is to adjust its rotational speed to the flow speed, as pointed out in a number of numerical works [10, 11, 12] mainly focused on the estimation of the best turbine rotational speed for different sea-states [12].

The aim of the present work is to perform an experimental test of a control strategy based on the turbine rotational speed, capable of maintaining the operating conditions as close as possible to the best efficiency point of the tested machine. Investigations were conducted in an OWC simulator housed at the Department of Mechanical, Chemical and Materials Engineering (DIMCM) in Cagliari, with the aim of applying the control strategy to the Wells turbine operating under deep stall conditions.

In the first part of this manuscript, the experimental setup is presented together with the instrumentation used and the related measurement uncertainties. In the second part, the performance parameters used to characterize the turbine are introduced and the control strategy is described in detail. Then, results are presented and discussed, while the last section draws some important conclusion.

2. OWC rig and instrumentation

Experimental tests have been conducted in an OWC simulator housed at the DIMCM, recently upgraded to simplify probe insertion for local flow investigation, by means of traverse measurements, and rotor assembly and disassembly. A scheme of this test rig is presented in Fig. 1.

The motion of the water surface inside an OWC system is simulated by moving a piston inside a steel chamber. A hydraulic unit allows several piston motion parameters, such as stroke amplitude, motion shape (triangular or sinusoidal) and period, to be modified. A linear wire potentiometer connected to the hydraulic unit allows the piston position to be feedback-controlled while recording its value during tests.

At the top of the chamber the Wells turbine is placed. Wall pressure taps, upstream and downstream of the rotor, are placed at different circumferential positions, in order to detect the

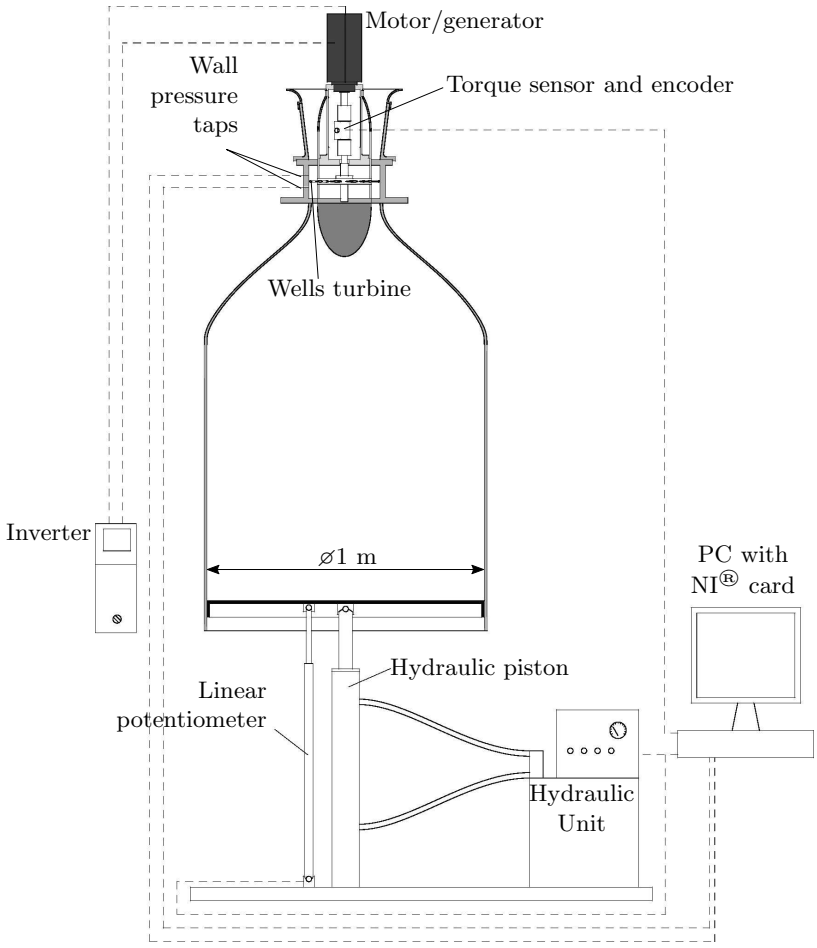

Figure 1. Simplified scheme of the experimental setup.

pneumatic averaged pressure. The Wells turbine, whose main dimensions are summarized in Tab. 1, is coupled to an induction motor, with a torque sensor and an encoder in between the two shafts. A voltage signal is sent to the inverter in order to set the rotational speed of the turbine.

Table 1. Geometric parameters of the Wells turbine.

rotor tip radius, r_{tip}	125 mm
rotor hub radius, r_{hub}	95 mm
tip clearance	1 mm
chord length, c	36 mm
number of blades, z	12
airfoil profile	NACA 0015
solidity	0.625
sweep ratio	0.417 (15/36)
hub-to-tip ratio, ν	0.76

Based on sensors' characteristics, calibration methods and uncertainty propagation, the expected measurements uncertainties are the following:

- 0.3% and 0.2% of full scale for the wall pressure measurements at ambient and piston side, respectively (the full scale is ±1 kPa for the ambient side transducer and ±7 kPa for the piston side one);
- 0.1% of sensor full scale (2 Nm) for the torque at the turbine's shaft;
- ±1 mm for the piston position.

Measurements' repeatability has been evaluated for the piston position and for the wall static pressure drop, which characterize the conditions the turbine operates at, and are the following:

- ±2.5 mm for the piston position;
- 0.6% of full scale of the piston side transducer for the pressure drop.

The current tests have been performed under sinusoidal piston motion as reproduced in Fig. 2 in non-dimensional form, by using the settings listed in Tab. 2.

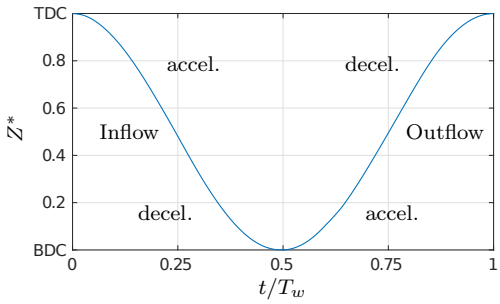

Figure 2. Shape of the piston motion set for the experiments.

A clarification of the nomenclature used for the phases of piston motion has been placed in Fig. 2.

Table 2. Setting of the experiments.

test reference id	**C9**	**C7**
turbine's reference rotational frequency, f	50 Hz	60 Hz
piston period, T_w	9 s	7 s
piston stroke amplitude	≈ 900 mm	≈ 900 mm
Reynolds' number of the relative outlet flow (based on the blade chord)	1.05×10^5	1.30×10^5

The operation settings in Tab. 2 have been selected in order to obtain deep stall conditions for the turbine, during both the inflow and the outflow phases. The aim of the experiments was to devise a control law capable to regulate the operating conditions in the turbine stable range, i.e. without stall, and as close as possible to the best efficiency condition.

All signals were acquired and generated (the control law) with a National Instruments NI® board, at the sampling frequency of 1 kHz.

3. Methodology

Wells turbine's global performance has been characterized considering typical non-dimensional parameters used in turbomachinery analysis:

$$\phi = \frac{C_z}{\Omega\, r_{tip}} \qquad T^* = \frac{T}{\rho\, \Omega^2\, r_{tip}^5} \qquad p^* = \frac{\Delta p}{\rho\, \Omega^2\, r_{tip}^2} \qquad \eta = \frac{T\, \Omega}{\Delta p\, Q} \tag{1}$$

where ϕ is the flow coefficient, T^* is the torque coefficient, p^* is the head coefficient and η is the turbine efficiency.

Due to the rig structure, it was not possible to use standardized instruments to measure the flow rate, Q. This was evaluated based on the piston motion, taking into account the time delay between the piston velocity and the corresponding flow speed at the rotor inlet, due to the presence of the chamber volume [13, 14, 15, 16].

3.1. Speed control approach

Each test has been divided in two phases: in the former, the *training* phase, the turbine was set to rotate at a constant speed for at least 5 piston periods and global variables (piston position, output torque, turbine rotational speed and wall-static pressure drop) were recorded. Based on the collected data, turbine performance were evaluated with a phase averaging of all the acquired signals. Considering the turbine pressure drop as one of the simplest measures, the head coefficient was assumed as representative of the operating conditions. In this way, considering that the maximum efficiency condition was obtained for $(p^*)_{opt}$, the control law required to set the angular velocity law for the turbine during a period was evaluated:

$$\Omega_{th} = \sqrt{\frac{\Delta p}{\rho\, (p^*)_{opt}\, r^2}} \tag{2}$$

Then, in the second phase, i.e. the *controlled* phase, this law was applied to the turbine. The control action was performed in a open-loop mode: the selected rotational speed temporal variation was applied, starting from a synchronization signal based on the piston motion. This type of control action has been preferred with respect to a feedback-controlled one, mainly to avoid too rapid control actions which can go beyond the inverter's capabilities and affect on torque sensor safety.

One should also note that the pressure drop through the rotor depends on the operating conditions the turbine works at, i.e the piston motion and the turbine rotational speed. It is reasonable to be expected that the control law established during the first *training* phase could not be the best one, due to the fact that the pressure drop distribution depends on the operating conditions. For this reason, the *training* process has been iteratively repeated, using the performance measured during the *controlled* phase as the input of a new *training* phase. As such, a new control law was established and successively applied to the turbine. This approach was repeated until the control law did not change significantly between two consecutive phases; then test was stopped.

At least 5 piston periods were acquired also during each *controlled* phase, after which all signals were processed with the phase averaging technique.

4. *Training* phase results

The instantaneous performance parameters for the turbine under stall are reported in Fig. 3, in non-dimensional form, for the two operating settings tested.

Figure 3 (a) clearly show that the conditions determined stall for both the two tests, with a drastic reduction in the value of the torque coefficient. In the stable range of operating conditions, for values of p^* between -0.5 and 0.5, no significant performance differences can

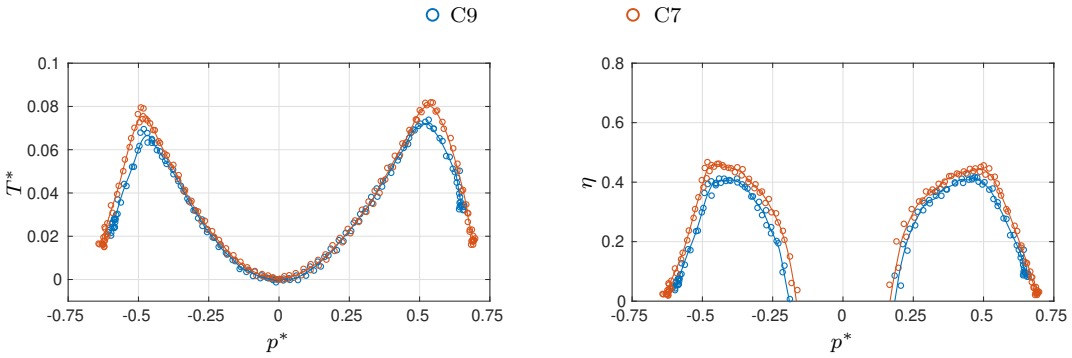

(a) Non-dimensional torque. (b) Efficiency.

Figure 3. Turbine's non-dimensional performance as a function of the head coefficient.

be observed between the two tests, except near the stall point: flow separation on the rotor happens for marginally higher values of ϕ for the C7 case, due to the larger Reynolds' number the turbine operates at, as reported in Tab. 2. Based on efficiency trends shown in Fig 3 (b), the best efficiency point was evaluated for the operating condition corresponding to a value of $(p^*)_{opt} = 0.46$. From this value of the head coefficient, Eqn. (2) was used to establish the control law, i.e. the rotational frequency variation, required to obtain the optimum value of p^*. Figure 4 reports the control law in terms of dimensionless frequency compared to the reference one, see Tab. 2, for each test.

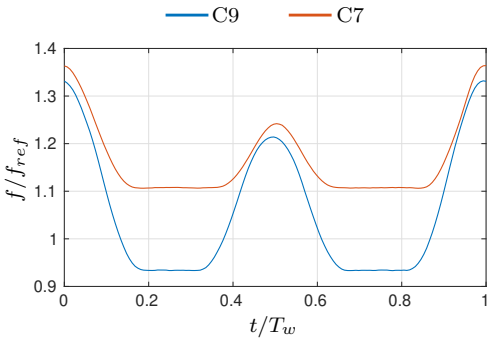

Figure 4. Applied rotational speed laws.

From Fig. 4, it is possible to observe that the control law takes into account the non-symmetric behavior of the Wells turbine coupled to the OWC system. In fact, during the outflow phase, the flow that comes from the chamber to the atmosphere is affected by a swirling component induced by the previous inflow phase [9, 13, 14, 17]. A polynomial approximation was used to smooth the control law deduced from measurements, in order to a) provide a law without the noise coming from the acquired signals and b) introduce a limit on the derivative term $\mathrm{d}f/\mathrm{d}t$, avoiding control actions which can overcome inverter and torque-sensor capabilities. The lower limit for the rotational speed needs to be introduced also to avoid near zero-rotational speed, would otherwise be expected at the piston inversion (when the flow axial velocity is low), and which acceleration and deceleration values.

5. *Control* phase results

Figure 5 compares the theoretical and applied laws for the C9 test case, for consecutive iterative loops. It should be noted several loops are required to find the optimal control law, as the

optimal conditions are a function of the pressure which is turns depends on the control strategy. The difference in the control law decreases between successive loops.

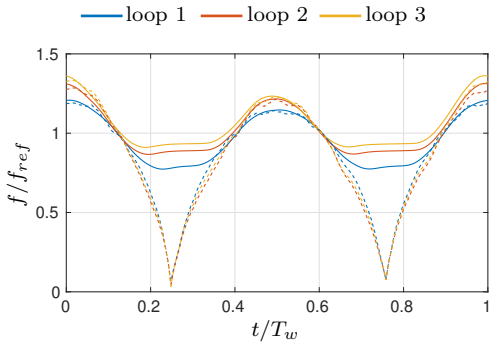

Figure 5. Theoretical (dashed line) and applied (solid line) control laws for the C9 test case.

After the first loop, the turbine was still stalled during the inflow phase, but this problem is solved in the following loops. At least three successive *training-control* loops were required to obtain the optimum control law. Test loops are shown only for the C9 test case, but very similar loops can be observed for the C7 one.

Performance obtained when the final control laws of Fig. 4 were applied are shown in Fig. 6.

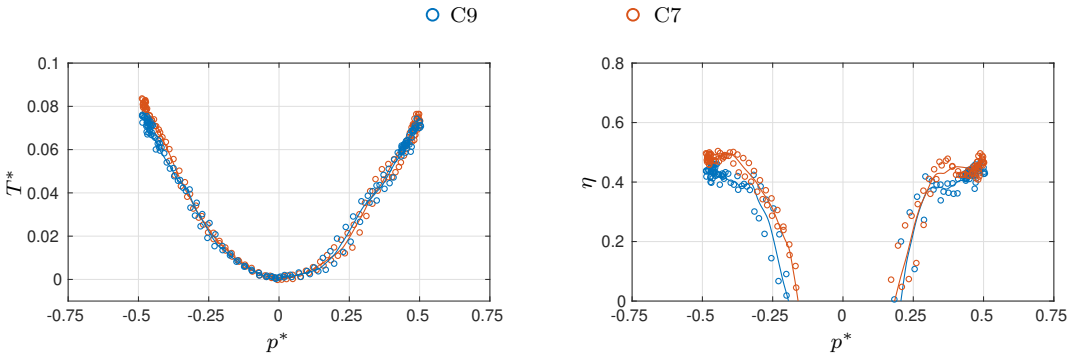

(a) Non-dimensional torque. (b) Efficiency.

Figure 6. Turbine's non-dimensional performance as a function of the head coefficient when the control law was applied.

Both Figs. 6 (a) and (b) clearly show the absence of stall, thus proving the effectiveness of the control strategy to obtain for the turbine operating conditions in the stable region. It should also be noted that the maximum value of the head coefficient for both tests, i.e. C9 and C7, is very close to the requested value for the best efficiency point ($p^* = 0.46$). This value is sometimes exceeded due to the dynamic response of the turbine to the control action, i.e. overshoots and undershoots in the turbine's actual rotational speed, but most of the values are effectively concentrated around $(p^*)_{opt}$. This important result can be better observed by looking at the frequency distribution of the operating conditions during a piston period, as shown in Fig. 7.

The bars in Figs. 7 (a) and (b) are very useful to observe how frequently the operating conditions are placed around the required value, when the rotor is controlled or not. This representation gives a better clarification of the effectiveness of the control strategy in moving the operating point of the turbine to the requested one.

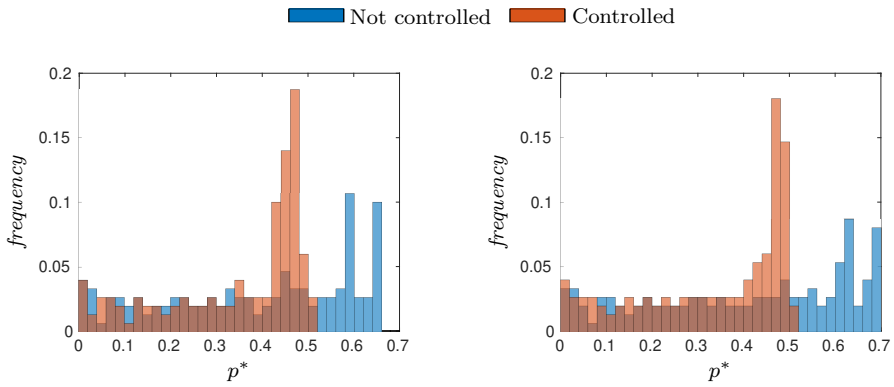

(a) Test C9. (b) Test C7.

Figure 7. Comparison of frequency distribution of operating conditions for the controlled and uncontrolled rotor, during both inflow and outflow phases.

Finally, it is also important to quantify the effectiveness of the control strategy in terms of turbine efficiency. To do this, it is helpful to evaluate the average efficiency during a piston cycle, which can be calculated as the ratio between the useful and the available energy, i.e. $\overline{\eta} = E_u/E_a$, following from Eqns. (3) and (4).

$$E_a = \int_{T_w} (\Delta p\, Q)\, \mathrm{d}t \tag{3}$$

$$E_u = \int_{T_w} (T\, \Omega)\, \mathrm{d}t \tag{4}$$

The resultant efficiency averaged on a cycle is then reported in Fig. 8.

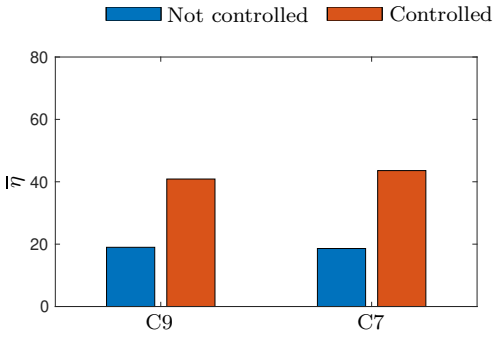

Figure 8. Turbine's average efficiencies during a cycle for the controlled and uncontrolled cases.

Efficiency improvements are noticeable, as both the initial tests start from stalled conditions at which the efficiency drop is relevant (see Fig. 6). The effectiveness of the control action with respect to the stalled conditions is evident, with an increase of about 100% for the turbine overall average efficiency. If the same speed control strategy is applied to the Wells turbine when the operating conditions are not affected by stall, efficiency improvements have been observed to be lower [18], in the order of 2-4%.

6. Conclusions

This work presents the experimental results for a speed-controlled Wells turbine coupled to an OWC simulator. A small-scale Wells turbine has been tested, under different piston/wave

periods, with the aim to verify the effectiveness of the control law proposed to a) avoid turbine stall under a selected wave motion and b) have the operating conditions as close as possible to the best efficiency point for most of the wave period.

An open-loop control strategy was chosen and applied iteratively in order to take into account that the pressure drop through the turbine, which was used to predict the control law, varies with the operating conditions. This type of control was selected not only to prevent control actions which can potentially overcome inverter and torque-sensor capabilities, but also as a reliable application in a real OWC plant where a *training* phase would be essential to make a good control prediction.

The results have shown the effectiveness of the control strategy, for both the initial requirements:

- the control law moves the turbine into its stable operating region, avoiding stall;
- the majority of the turbine's operation is close to its best efficiency point.

The authors do not exclude that a control strategy designed ad-hoc could increase the benefits, especially to obtain more frequently the optimal operating conditions and to mitigate the overshoots and undershoots on the actual turbine rotational speed. Future investigations could be performed to verify the effectiveness of the proposed control strategy for adapting the turbine rotational speed to non-regular waves and to different sea-states that occur during operations of OWC devices with Wells turbines.

References

[1] R. Pelc and R.M. Fujita. Renewable energy from the ocean. *Marine Policy*, 26(6):471–479, 2002.
[2] A. F. O. Falcão. Wave energy utilization: A review of the technologies. *Renewable and Sustainable Energy Reviews*, 14(3):899–918, 2010.
[3] A. F. O. Falcão and J. C. C. Henriques. Oscillating-Water-Column wave energy converters and air turbines: A review. *Renewable Energy*, 85:1391–1424, 2016.
[4] A. A. Wells. Fluid Driven Rotary Transducer - BR. Pat. 1595700, 1976.
[5] S. Raghunathan, C. P. Tan, and O. O. Ombaka. Performance of the Wells self-rectifying air turbine. *Aeronautical Journal*, 89:369–379, December 1985.
[6] L. M. C. Gato and A. F. O. Falcão. Aerodynamics of the Wells turbine. *International Journal of Mechanical Sciences*, 30(6):383 – 395, 1988.
[7] M. Takao and T. Setoguchi. Air turbines for wave energy conversion. *International Journal of Rotating Machinery*, 2012, 2012.
[8] S. Raghunathan. The Wells air turbine for wave energy conversion. *Progress in Aerospace Sciences*, 31(4):335–386, 1995.
[9] F. Licheri, P. Puddu, T. Ghisu, and F. Cambuli. Experimental analysis of the unsteady flow inside a Wells turbine. *Proceedings of the 76th Italian National Congress ATI*, 312:11009, 2021.
[10] M. Amundarain, M. Alberdi, A.J. Garrido, I. Garrido, and J. Maseda. Wave energy plants: Control strategies for avoiding the stalling behaviour in the Wells turbine. *Renewable Energy*, 35(12):2639–2648, 2010.
[11] O. Barambones, J.A. Cortajarena, J.M. Gonzalez de Durana, and P. Alkorta. A real time sliding mode control for a wave energy converter based on a Wells turbine. *Ocean Engineering*, 163:275–287, 2018.
[12] J. Lekube, A.J. Garrido, and I. Garrido. Variable speed control in Wells turbine-based oscillating water column devices: Optimum rotational speed. *Proceedings of the 6th International Conference on Power Science and Engineering ICPSE2017*, 136(1), 2018.
[13] P. Puddu, M. Paderi, and C. Manca. Aerodynamic characterization of a Wells turbine under bi-directional airflow. *Proceedings of the 68th Italian National Congress ATI*, 45:278–287, 2014.
[14] M. Paderi and P. Puddu. Experimental investigation in a Wells turbine under bi-directional flow. *Renewable Energy*, 57:570–576, 2013.
[15] T. Ghisu, P. Puddu, and F. Cambuli. Physical explanation of the hysteresis in Wells turbines: A critical reconsideration. *Journal of Fluids Engineering, Transactions of the ASME*, 138(11), 2016.
[16] T. Ghisu, F. Cambuli, P. Puddu, I. Virdis, M. Carta, and F. Licheri. A lumped parameter model to explain the cause of the hysteresis in OWC-Wells turbine systems for wave energy conversion. *Applied Ocean Research*, 94:101994, 2020.

[17] T. Ghisu, P. Puddu, and F. Cambuli. A detailed analysis of the unsteady flow within a Wells turbine. *Proceedings of the Institution of Mechanical Engineers, Part A: Journal of Power and Energy*, 231(3):197–214, 2017.

[18] F. Licheri, P. Puddu, F. Cambuli, and T. Ghisu. Experimental investigation on a speed controlled Wells turbine for wave energy conversion. *Proceedings of the 41st International Conference on Offshore Mechanics and Arctic Engineering*, (in press), 2022.